Review Article

Shufang Zhu, Xin Meng, Xu Yan*, and Shaojuan Chen

# Evidence for bicomponent fibers: A review

https://doi.org/10.1515/epoly-2021-0067
received June 18, 2021; accepted July 29, 2021

**Abstract:** Recently, bicomponent fibers have been attracting much attention due to their unique structural characteristics and properties. A common concern was how to characterize a bicomponent fiber. In this review, we generally summarized the classification, structural characteristics, preparation methods of the bicomponent fibers, and focused on the experimental evidence for the identification of bicomponent fibers. Finally, the main challenges and future perspectives of bicomponent fibers and their characterization are provided. We hope that this review will provide readers with a comprehensive understanding of the design and characterization of bicomponent fibers.

**Keywords:** bicomponent fibers, classification, structural characteristics, preparation, identification

## 1 Introduction

Synthetic fibers based on polymers have been developed for about 100 years. During these times, different types of fibers were fabricated and applied in various fields. With the expansion of production scale and increasingly fierce market competition, the development of synthetic fibers has entered a stage wherein the focus of development has shifted from "quantity" to "quality" and from conventional products to new products from the 1960s. Within this framework, differential fibers have attracted a lot of interest, especially the bicomponent fibers (1–9). The original intention of preparing bicomponent fibers was to achieve wool fiber-like structure and self-crimping effect, and this concept was first proposed in the 1940s, and was first commercialized in the mid-1960s (10). With the development of dissolved composite fibers in Japan in the 1970s and the appearance of core/shell fibers as well as the "ultrafine heat" set off by the emergence of textiles spun from ultrafine fibers such as leather-mimicking and silk-mimicking products in the international textile market further promoted the development of bicomponent fibers. Moreover, the raw materials and types of bicomponent fibers were also further supplemented and expanded, the raw materials changed from a single type to a mixture of multiple types, and the cross-sectional shape also expanded from the common cross-sectional shape to an irregular shape.

Generally, the bicomponent fibers belonged to a type of composite fiber, also known as "conjugated fiber", which referred to the fibers formed by two different polymers fed into different spinning channels in the form of melt or solution, respectively, and finally extruded from the same nozzle hole (11–13). Bicomponent fibers with different cross-sections could be prepared from different shapes of the spinneret, and the preparation methods of bicomponent fibers were diverse, and mainly included spun bonding, electrospinning, melt-blowing, and gel spinning. Through these methods, the advantages of the two raw materials were combined, so as to obtain fibers with various properties (14). The emergence of these bicomponent fibers with excellent properties not only enriched the types of fibers but also advanced the quality of the prepared textiles, thus attracting the attention of many scientific researchers (15–27). At present, the production technology of bicomponent fibers is mainly focused on the filament, staple fibers, and heat-bonded nonwoven fabrics, and its application also widely involves the fields of medicine, energy, and clothing (28–33). The importance of bicomponent fibers is gradually increasing due to their multiple uses.

Actually, the structures and component materials of the bicomponent fibers were determined by the preparation methods. However, to identify their structures and components, different types of methods were used that

* **Corresponding author: Xu Yan,** Industrial Research Institute of Nonwovens and Technical Textiles, Shandong Center for Engineered Nonwovens, College of Textiles and Clothing, Qingdao University, Qingdao 266071, China; Collaborative Innovation Center for Eco-Textiles of Shandong Province, Qingdao University, Qingdao 266071, China; State Key Laboratory of Bio-Fibers and Eco-Textiles, Qingdao University, Qingdao 266071, China,
e-mail: yanxu-925@163.com
**Shufang Zhu, Xin Meng, Shaojuan Chen:** Industrial Research Institute of Nonwovens and Technical Textiles, Shandong Center for Engineered Nonwovens, College of Textiles and Clothing, Qingdao University, Qingdao 266071, China

could be directly observed by the microscope and energy dispersive spectrometer (EDS) analysis. However, there are few literature studies to discuss the evidence for the bicomponent fibers.

In this review, we first discussed the definition of the bicomponent fibers in Section 2, and then in Section 3 the preparation methods of bicomponent fibers with different structures were summarized. In Section 4, we mainly focused on the identification of bicomponent fibers and how to distinguish these different structures. Finally, a conclusion and perspectives were provided.

# 2 Classification of bicomponent fibers

## 2.1 Classification

There were a wide variety of bicomponent fibers, which could be classified differently according to different standards. According to the composition of polymer materials, they might be divided into three categories: polyethylene (PE)/polypropylene (PP), PP/polyethylene terephthalate (PET), high-density polyethylene/low-density polyethylene, etc. (34–38). According to the cross-sectional shape, they could be generally divided into three categories: side-by-side type, core/shell type, and matrix/protofibril type, etc., and their shapes are shown in Table 1 (39–41). These types were also introduced in detail according to the classification of the fiber section below.

### 2.1.1 Side-by-side bicomponent fibers

Side-by-side fibers referred to the fiber made from two kinds of polymers with different shrinkages or melt viscosities distributed in adjacent states along the fiber axis, and the original purpose was to imitate the curled and fluffy structure of wool (43–45). According to the difference of side-by-side mode between the two components, it could be divided into side-by-side, side-by-side hollow, and side-by-side eccentric hollow types. The side-by-side type not only had a common double-layer side-by-side type but also had a multilayer side-by-side type and a triangular side-by-side type. The most important feature of side-by-side bicomponent fibers was that they could produce permanent three-dimensional curling due to the following reasons (46):

(1) the cross-sectional shape of the fibers, as well as the independent cross-sectional shape of the two components, was different;
(2) the bicomponents had different modulus;
(3) shrinkage differences between two components;
(4) the different fineness of fibers; and
(5) the two polymers had different composite ratios and melt viscosities.

Side-by-side bicomponent fibers used different shrinkage rates of the two components and asymmetric distribution of

**Table 1:** Schematic diagram of the bicomponent fiber

| Species of bicomponent fibers | Cross section of bicomponent fibers |
|---|---|
| Side-by-side |  |
| Core/shell |  |
| Matrix/protofibril | Islands-in-the-sea |
| |  |
| | Segmented-pie |
| |  |

Reprint with permission (42) Copyright 2013, Elsevier Ltd.

sections to obtain permanently contracted three-dimensional crimped fibers when subjected to stretching or heat treatment, which can increase the bulkiness, heat preservation, and softness of the fabric (47–52). For example, Yan et al. (53) used polytrimethylene-terephthalate (PTT) and low-viscosity PET as raw materials to prepare side-by-side bicomponent fibers with good curling performance by spinning technology using the difference in shrinkage properties between the two components.

However, the two components in side-by-side bicomponent fibers need to meet certain compatibility, and the difference in composition between the two components should not be too large, otherwise, they might be separated and would not form a component state due to insufficient adhesion between the two components resulting in the inability to withstand excessive mechanical force during processing.

#### 2.1.2 Core/shell bicomponent fibers

The core/shell bicomponent fibers consisted of two independent fiber chambers; the inner compartment "core" was completely surrounded by the outer one "shell" (54,55). In the core/shell bicomponent fibers, the adhesive force between the two components was not the main force, and the mechanical connection was generated by using the surrounding interface between the shell and the core. This interface played a certain bonding role and then avoided splitting during processing. The target function of the core/shell bicomponent fibers was clear, i.e., the shell mainly provided the surface properties of bicomponent fiber, such as luster, thermal adhesion, hygroscopicity properties, and dyeing properties (56–61). The core material could be a material with a wide range of sources, low cost, high strength, and stable performance, so it could provide better mechanical properties and achieve the purpose of reducing costs (62–67). A very important advantage of the core/shell bicomponent fiber was that it could help a material that could not be spun into a fiber single form as the core component. For example, Sun et al. (68) successfully prepared PEO/PDT core/shell bicomponent fibers by co-electrospinning for the first time and observed the obvious core/shell structure under a microscope. However, in this experiment, PDT could not only form a fiber due to its low molecular weight, but also form fiber through the role of PEO as a template to promote its molding. Therefore, the appearance of the core/shell bicomponent fibers improved the spinnability and performance of the fibers.

#### 2.1.3 Matrix/protofibril bicomponent fibers

Matrix/protofibril bicomponent fibers mainly included islands-in-the-sea (INS) type and segmented-pie type. INS fiber, also known as ultraconjugated fiber, had two forms of filament and staple fiber, and it was composed of "island" formed by one component dispersed in "sea" formed by the other component (69); segmented-pie bicomponent fiber was composed of two kinds of polymers with close viscosities but incompatibility, which passed through the spinning assembly separately, pooled before the nozzle hole, and finally ejected by the nozzle hole for cooling/molding so that the fiber with a section similar to the shape of segmented-pie was formed (70). Since the interfacial force of the two components of matrix/protofibril fibers was not strong and incompatible with each other, when the INSbicomponent fibers or interphase distributed segmented-pie bicomponent fiber formed fabrics, the two components were separated by chemical or physical methods to obtain microfibers. Consequently, the as-spun fibers were applied in the field of adsorptive materials, sound-absorbing materials, or leather. Once the island components were dissolved to obtain porous hollow fibers, then the sea components could be microfined by expansion to increase the heat preservation of fabrics (71–78).

## 3 Preparation of bicomponent fibers

To obtain bicomponent fibers with different structures, the selection of raw materials, spinning equipment, and composite spray assemblies were the most important factors. In this section, the preparation methods of different types of bicomponent fibers were summarized briefly.

### 3.1 Side-by-side bicomponent fibers

The basic principle for the production of side-by-side bicomponent fibers was that the two polymer melts or solutions reached the separated nozzle holes with a separator or knife-edge, and finally, flowed in the nozzle hole in a side-by-side form. The general preparation methods included the melting spinning method (79) and electrospinning method (80–85), and the specific preparation processes are listed as follows (86):

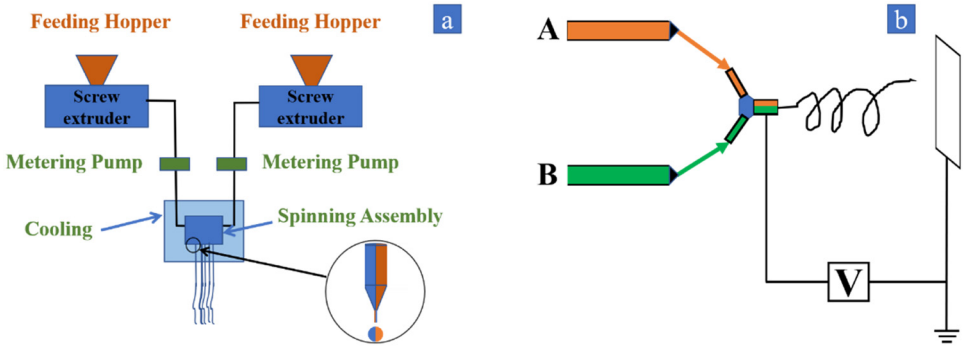


**Figure 1:** Schematic diagram of the preparation of side-by-side bicomponent fibers by direct feeding: (a) melt spinning and (b) electrospinning (87).

(1) One of the most commonly used ways to produce side-by-side bicomponent fibers was direct feeding, in which the two components were fed directly into the nozzle assembly in the form of a solution or melt, and finally, merged near the nozzle to form bicomponent fibers, as shown in Figure 1. Particularly, for the electrospinning methods, it mainly depended on the side-by-side spinneret to form a side-by-side bicomponent fiber.
(2) The two components also could form a multilayer structure first, and then fed into the navigate nozzle at a lower speed without turbulent interference, so that the polymer penetrated through the internal interface of each interlayer and formed a multilayer cross interface.
(3) The two components first formed a multilayer structure, but the nozzle did not run through the inner interface, which could prepare fibers with a large range of composite states whose components could be arbitrarily partitioned from 0% to 100%.
(4) The two polymer slicing components were extruded into a multilayer film, followed by the slider, stretched to improve polymer orientation, then through the carding machine for fibrillization, and finally, through thermal shrinkage to improve coiling.
(5) The two components in the molten state were pooled on a roller with a V-shaped grooved cylinder, and after extrusion and stretching of a group of rollers, the two components could be bonded together in a side-by-side mode and then followed by elastic treatment to have ideal mechanical curling.

## 3.2 Core/shell bicomponent fibers

Generally, there were two types of core/shell fibers: concentric and eccentric bicomponent fibers. Concentric bicomponent fibers almost could not curl spontaneously; otherwise, most of the eccentric fibers could curl spontaneously (88–90). The core/shell fibers could be prepared by melt spinning as suggested in Figure 2a (91,92), electrospinning as shown in Figure 2b (9,93–97), and gel spinning (98), as listed in Table 2 (99).

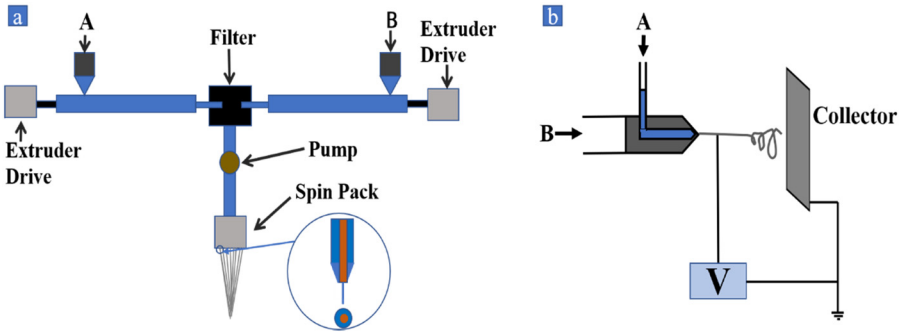


**Figure 2:** Schematic diagram of the preparation of core/shell bicomponent fibers: (a) spun bonding and (b) electrospinning. (a) Adapted with permission (91) Copyright 2011, Springer Science Business Media; (b) adapted with permission (100) Copyright 2004, American Chemical Society.

**Table 2:** Fabrication of core/shell bicomponent fibers

| Core/shell fibers | Eccentric core fibers |
|---|---|
| (1) A liquid or melt of both polymers was introduced into the vicinity of the nozzle and then extruded according to the core shape<br>(2) The fiber was coated by another polymer melt<br><br>(3) During spinning of the core polymer, a water latex solidification bath containing another polymer is used | (1) Adjusting variable factors such as the location of channels inside the polymer, the output rate of the two polymer components, etc.<br>(2) Before the concentric core/shell component comes out of the nozzle, a separate group shunt was introduced to merge with it<br>(3) Deform the concentric fiber through a hot knife-edge |

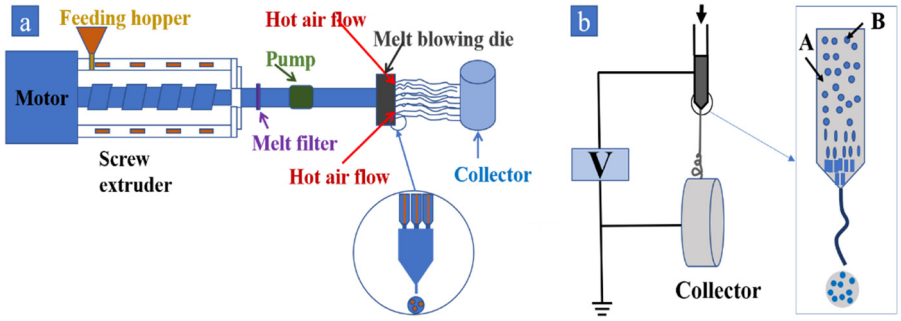


**Figure 3:** Schematic diagram of the preparation of islands-in-the-sea bi-component fibers: (a) melt blowing and (b) electrospinning. (a) Adapted with permission (108) Copyright 2019, The Korean Fiber Society; (b) adapted with permission (109) Copyright 2007, American Chemical Society.

### 3.3 Matrix/protofibril bicomponent fibers

The main methods to produce INSbicomponent fibers were melt blowing as shown in Figure 3a (101–103) and electrospinning (Figure 3b) (104), and the main methods to prepare segmented-pie bicomponent fibers were melt spinning as shown in Figure 4 (105–107).

There were two main processing principles for the production of INS fibers: in the first one, the two polymer fluids formed a composite fine flow in the form of core/shell or side-by-side mode, and then they were pooled together. One of the polymers existed in the other polymer melt in the form of suspended droplets and after spraying and stretching treatment, the dispersed droplets could be stretched into microfibers parallel to the axial direction of the fibers, and finally, the obtained bicomponent fibers were treated according to the application needs (110). In the second one, one polymer was blended with another polymer in the form of microspheres, and INS fibers could be obtained by stretching under high temperature and speed air flow during spinneret (108).

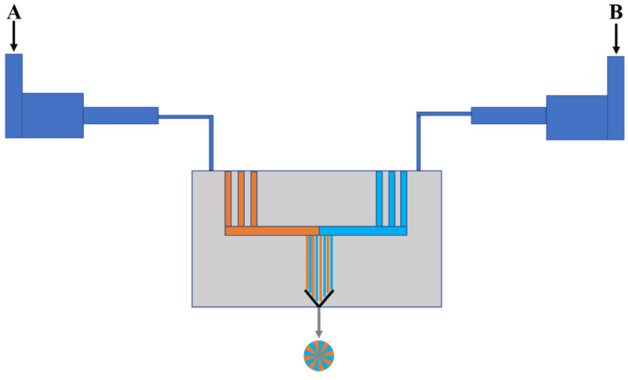


**Figure 4:** Schematic diagram of the preparation of segmented-pie fibers by the melt-spinning process.

## 4 Identification of bicomponent fibers

There were many patterns of bicomponent fibers and various types of combinations, which caused difficulties in identifying their composition and structure to some extent. Bicomponent fibers were different from other chemical fibers. In general, since the two components of bicomponent fibers did not undergo a chemical reaction, they were only combined in a physical way. Therefore, the identification of their categories included not only the types of

their constituent fibers but also the structural types. Here, we summarized the reported methods to examine the bicomponent fibers from structures and component analysis.

## 4.1 Structure evidence for bicomponent fibers

### 4.1.1 Direct identification with a microscope

Microscopic observation using a microscope to observe the cross-section of fibers directly was the most common method to identify the structure of bicomponent fibers. Since different components had different refractions to light, they would present different colors under the microscope, so as to judge the position distribution of the two components.

Previously, microscopic observation was performed using optical microscopy. For example, Ayad et al. (111) prepared side-by-side bicomponent fibers by melt spinning using PP and PA6 as raw materials and characterized their structural characteristics using optical microscopy. As shown in Figure 5a, the fibers showed interfacial irregularities and the two components presented a side-by-side morphology, both with an external boundary. Cherif et al. (112) prepared core/shell bicomponent fibers by the melt-spinning technique using PP as the shell material; PP and phase change material (PCM) co-mixes as the core material and then the structure was characterized using an optical microscope. From Figure 5b, it can be seen that the components with PCM and PP mixture as the core were firmly surrounded by PP shell components, and the inner and outer layers were clearly demarcated. Shu and Hsiao (113) used polytrimethylene terephthalate (PTT) as the "island" component and metallocene isotactic polypropylene (m-iPP) as the "sea" component to prepare INS PTT/m-iPP bicomponent microfilaments by conjugate spinning. It can be seen from Figure 5c that the "island" components showed a dispersed phase structure and were dispersed in the "sea" component composed of PTT and the two components were incompatible with each other. Zhao and Liu (114) used PA6 and PET as raw materials to prepare PA6/PET segmented-pie bicomponent fibers by spun bonding process and characterized them by using an optical microscope. It can be seen from Figure 5d that the two components presented a segmented-pie shape, the interface was clear, and there was no mutual extrusion of components.

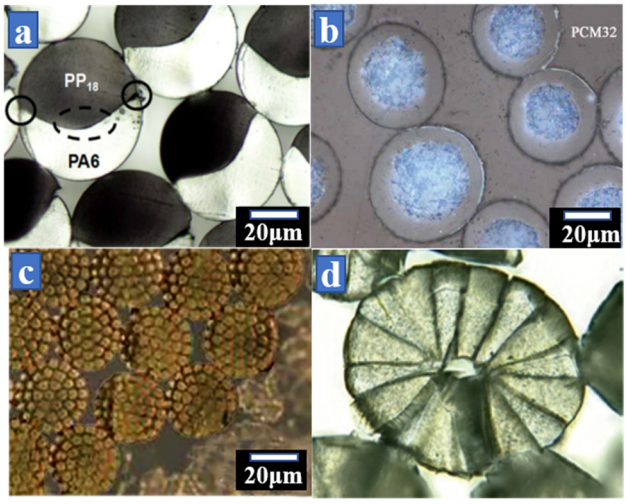


**Figure 5:** Cross-section of the fiber characterized by optical microscopy: (a) side-by-side bicomponent fiber with 50 wt% $PP_{18}$/50 wt% PA6, (b) core/shell melt-spun PCM32 bi- fibers, (c) islands-in-the-sea PTT/m-iPP (75/25) conjugated filaments, and (d) segmented-pie PA6/PET bicomponent fiber (×1,000). (a) Reproduced with permission (111) Copyright 2016, ASM International; (b) adapted with permission (112) Copyright 2018, Express Polymer Letters; (c) adapted with permission (113) Copyright 2007, Springer Science Business Media B.V; (d) adapted with permission (114) Copyright 2012, Zhao and Liu.

Besides, electron microscopy also could be used for microscopic observation of the bicomponent fibers, including SEM and TEM observation. Im et al. (115) prepared core/shell polyvinyl alcohol (PVA)/zirconia ($ZrO_2$) bicomponent nanofibers by electrospinning technique and examined the bicomponent nanofibers structure using SEM. From Figure 6a, it can be seen that the core/shell structure was well-formed, and the shell material (white) was wrapped with the core material (black). Yeom and Pourdeyhimi (116) used PA6 as the "island" material and PE as the "sea" material to prepare INS fibers by bicomponent spun-bonding technology, and characterized their cross-sectional morphology using SEM. As shown in Figure 6b, PA6 was evenly dispersed in PE, and there was an interface between the "sea" component and the "island" component. Zhao et al. (117) prepared a hollow segmented-pie bicomponent fiber by the multifluid compound jet electrospinning technique with $Ti(OiPr)_4$ and poly(vinyl pyrrolidone) as external solutions and paraffin oil as internal solutions and then calcined the obtained fiber to obtain a $TiO_2$ three-channel tube ($TiO_2$ TCT), which was characterized by SEM. The microstructure of the fiber is shown in Figure 6c; the whole fiber presented a hollow structure, the fiber interior was divided into three cavities by Y-shape, and the section presented a segmented-pie shape.

TEM was also an effective way to identify the structures of bicomponent fibers (118–120). For example, Rajgarhia et al. (121) used polyvinyl acetate (PVAC) and polyvinyl pyrrolidone (PVP) as materials to prepare

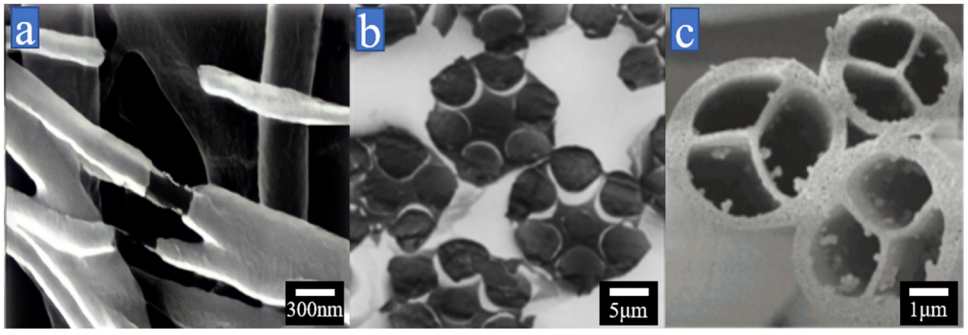


**Figure 6:** SEM images of (a) core/shell PVA/$ZrO_2$ composite nanofibers, (b) INS web with several numbers of islands in the sea, and (c) hollow segment-pie bicomponent fibers. (a) Adapted with permission (115) Copyright 2014, The Korean Fiber Society and Springer Business Media Dordrecht; (b) adapted with permission (116) Copyright 2011, Springer Science Business Media, LLC; (c) reproduced with permission (117) Copyright 2007, American Chemical Society.

side-by-side bicomponent fibers by vaporization-induced polymer phase separation using the gas jet fiber (GJF) method. To characterize the fiber structure, the TEM image was taken as shown in Figure 7a; a side-by-side fiber can be seen clearly with a double spherical morphology, and half of the fiber cross-section was occupied by PVAc and the other half by PVP, reflecting a 1:1 wt/wt ratio of the two polymers in the starting solution. Moreover, PVP appeared darker in the image due to the higher electron density compared to PVAc. The side-by-side structure was also confirmed by selectively dissolving water-soluble PVP in deionized water for 6 h at room temperature. Nguyen et al. (122) prepared poly(lactic acid) (PLA)/chitosan (CS) core/shell bicomponent nanofibers by coaxial electrospinning and characterized their structures using TEM. As shown in Figure 7b, due to the difference in the density of the core and shell material, the contrast difference of the core and shell was obtained and it could be seen that the PLA core was completely wrapped by the CS shell and the interface between the shell and the core was clearly observed.

In addition to the observation using a single type of microscope, it could also use the combination of two types of microscopes to identify the bicomponent structure more clearly and intuitively (123). For example, Gernhardt et al. (124) clearly observed the side-by-side structure of poly(*N*-isopropylacrylamide) (PNiPAAm)/methyl methacrylate and butyl methacrylate (P(MMA-*co*-BMA)) bicomponent fibers by the combination of TEM and Raman/AFM. As shown in Figure 8a and b, the bicomponent fibers presented asymmetric side-by-side structures.

### 4.1.2 Direct identification by fluorescent labeling

To avoid the fact that the two-component materials were not sensitive to light, fluorescent labeling methods were selected as an effective method to identify the bicomponent fiber structures. The principle of fluorescence labeling was that when the fluorescent substance was irradiated with light, the fluorescent substance absorbed the energy of light consistent with its characteristic frequency. Then it transits from the ground state to the excited state and emit fluorescence when it dropped from the lowest vibration energy level of the first excited state to the original ground state (125).

Lee et al. (126) selected polythiophene polymers (PDS306PT and ADS406PT) as photoluminescent red and

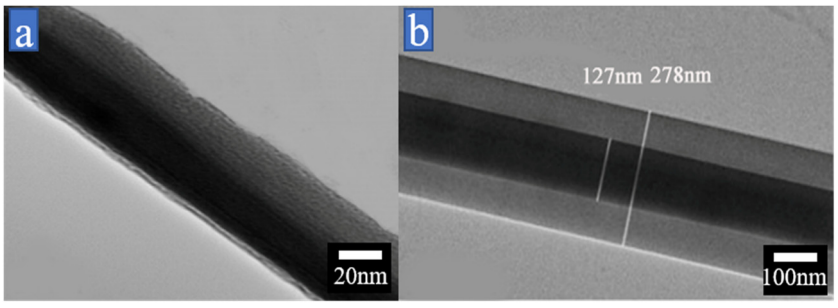


**Figure 7:** TEM images of (a) side-by-side PVAc/PVP fibers and (b) core/shell PLA/CS nanofibers. (a) Adapted with permission (121) Copyright 2016, Elsevier Ltd.; (b) adapted with permission (122) Copyright 2011, Elsevier Ltd.

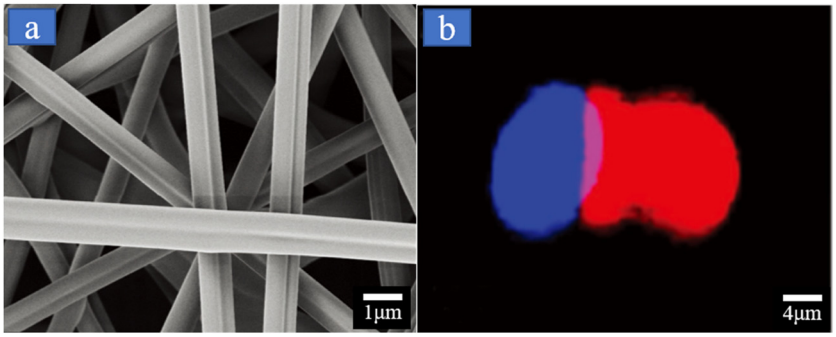


**Figure 8:** SEM image and AFM topography image of side-by-side bicomponent fibers made from P(MMA-*co*-BMA) and PNiPAAm (a) SEM image and (b) Roman cross-section of the side-by-side bicomponent fibers. Adapted with permission (124) Copyright 2017, WILEY-VCH Verlag GmbH & Co. KGaA, Weinheim.

blue dyes and blended them into poly(lactide-*co*-glycolide)-oly(vinyl cinnamate) (PLGA-PVCi) and poly(vinyl cinnamate) (PVCi), respectively, and fabricated side-by-side PLGA-PLGA/PVCi bicomponent fibers by the electrohydrodynamic (EHD) co-spray method. The fiber structures were characterized by confocal laser scanning microscopy (CLSM). From Figure 9a, one can observe that the cross-sectional CLSM image of the biphasic microfibers presents two different colors: blue and red, showing the obvious boundary of side-by-side fibers, distributed on both sides of the fibers. Jin et al. (127) prepared PCL/PVP side-by-side bicomponent nanofibers by electrospinning by adding fluorescent dyes coumarin (green) and rhodamine B (red) to PCL and PVP solutions, respectively. The structure of the as-spun fiber was examined by CLSM. As shown in Figure 9b, the PVP fibers presenting red were arranged parallel to the PCL fibers with green, and there was a clear color boundary between the two single-component fibers. Similarly, Lee et al. (128) prepared poly(lactide-*co*-glycolide)/thermal cross-linkable polymer/poly(lactide-*co*-glycolide) (PVCi/ER/PLGA) Janus core/shell fibers using PLGA as the shell and PVCi/ER as the core through double-core flow coaxial co-wetting and characterized them using CLSM. Figure 8c shows the cross-sectional CLSM image of the double-core core/shell fiber. From Figure 9c, it can be seen that all fibers contained two parallel cores, the cores were blue and green, and the shell was light black due to the addition of blue fluorescent to PVCi and green fluorescent to ER. In addition, clear boundaries between individual cores and between the cores and shell confirmed the internal core/shell structure of the microfiber.

### 4.1.3 Infrared chemical imaging

Infrared chemical imaging was also one of the common methods to identify the structure of the bicomponent fibers. Infrared chemical imaging combined traditional chemical imaging and infrared spectroscopy methods and had the advantages of both. Infrared chemical imaging could spatially distinguish two spectrally different regions, and infrared spectroscopy can be used to identify the overall chemical composition of fibers. A major disadvantage of infrared technology was that the spatial structure of fibers needs to be known before infrared analysis. Infrared chemical imaging can fully characterize bicomponent

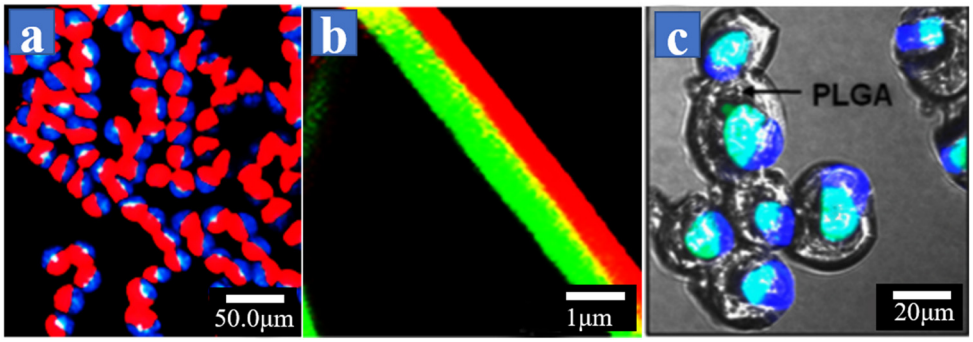


**Figure 9:** CLSM images of (a) PLGA-PLGA/PVCi side-by-side bi-component fiber, (b) PVP/PCL side-by-side fiber, and (c) PVCi/ER core/PLGA shell microfibers. (a) Adapted with permission (126) Copyright 2010, Wiley-VCH GmbH & Co. KGaA; (b) adapted with permission (127) Copyright 2014, Springer Science Business Media New York; (c) adapted with permission (128) Copyright 2013, American Chemical Society.

fibers, enabling the simultaneous collection of hundreds to thousands of infrared spectra from the entire sample to potentially reveal any inhomogeneity present in the sample. A number of different infrared sampling methods were used to analyze each two-component fiber sample, including normal transmission analysis and two microsampling techniques.

Flynn et al. (129) characterized the structure of polyurethane/nylon side-by-side fibers by infrared chemical imaging. From Figure 10, it can be seen that the infrared chemical image formed by imaging the integrated spectral intensity under peaks centered near 1,641 $cm^{-1}$ (amide I in polyamide) and 1,735 $cm^{-1}$ (carbonyl stretching in polyurethane), clearly revealed that this sample not only consisted of two components, but also its spatial configuration was a side-by-side bicomponent fiber (in Figure 10a), and the two components were clearly distinguished. The infrared spectrum of each component was obtained by clicking one pixel on each side, and the infrared spectra of each component are shown in Figure 10b and c, where Figure 10b is the infrared spectrum of nylon, corresponding to the red part in Figure 10a, and Figure 10c is the infrared spectrum of polyurethane, corresponding to the blue part in Figure 10a.

## 4.2 Component evidence for bicomponent fiber

### 4.2.1 EDS analysis for bicomponent fiber

Energy dispersive spectrometry (EDS) was also believed to be a useful way to distinguish the different components in a bicomponent fiber. EDS analytical methods included point analysis, line scan analysis, and surface distribution, and different analytical methods had different characteristics. The point analysis was mainly performed by fixing the probe on the point of interest of the sample for quantitative and qualitative analysis; the linear scanning analysis could visually display the distribution of elements in different phases or regions; and the surface distribution was mainly shown by the distribution of elements on the sample surface in the luminance distribution on the screen, which was usually used for the distribution of impurities and phases in the material and elemental segregation. Consequently, EDS could be applied to the identification of the bicomponent fiber structure.

Chen et al. (130) prepared Janus nanofibers from polyvinylpyrrolidone K60 (PVP K60)/rhodamine b and Eudragits® L100/8-anilino-1-naphthalenesulfonic acid ammonium salt (EL100/ANS-NH4) by a side-by-side electrospinning process and characterized them by EDS. As shown in Figure 11a(I), three points (A, B, and C) were selected for EDS analysis and the results were shown in Figure 11(a(II)–(IV)). An amount of 0.6 wt% sulfur detected in the analysis shown in Figure 11a(II) indicated that the A point was on one side of EL100/ANS-NH4. While the presence of chlorine in the spectrum shown in Figure 11a(III) indicated that point B was on the side of PVPK60/rhodamine b, and the spectrum of point C in Figure 11a(IV) showed the coexistence of sulfur and chlorine because it was the result of the transverse topology of the entire Janus nanofiber. Liu et al. (131) prepared side-by-side $TiO_2/SnO_2$ bicomponent fibers through a side-by-side double-spinneret electrospinning setup and characterized the elemental distribution of the as-spun fiber using EDS. The EDS analysis of the nanofibers is shown in

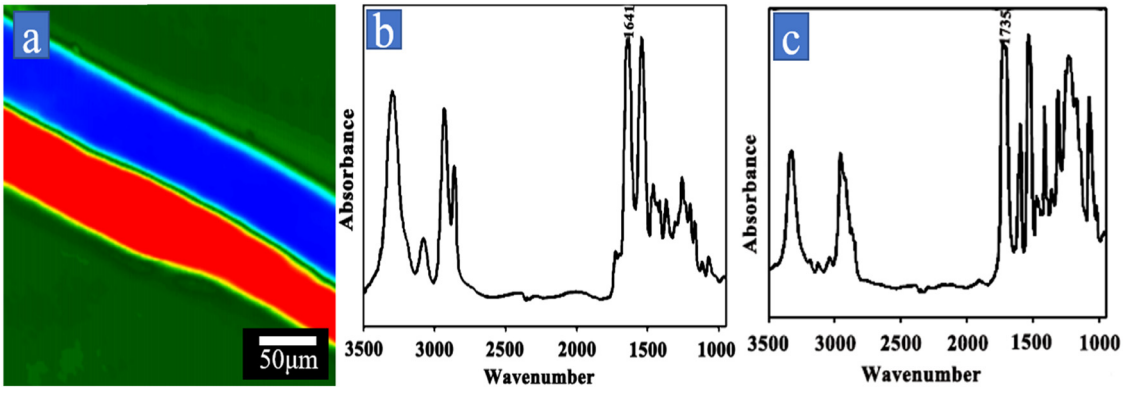


**Figure 10:** (a) Infrared chemical image of polyurethane/nylon bicomponent fiber formed by imaging at 1,641 and 1,735 $cm^{-1}$, (b) infrared spectrum of the red part, identified as nylon, and (c) infrared spectrum of the blue part, identified as polyurethane. (a–c) Adapted with permission (129) Copyright 2006, American Academic of Forensic Sciences.

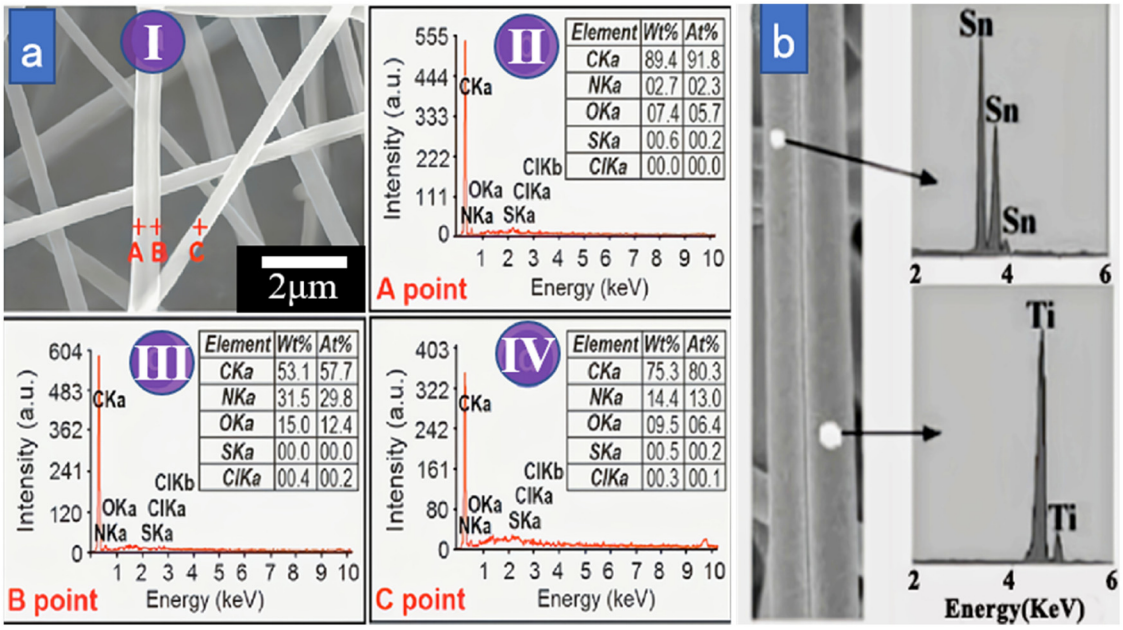


**Figure 11:** (a) Janus PVP K60/rhodamine b and EL100/ANS-NH4 fiber, where I is field emission scanning electron microscopy FESEM image of the Janus nanofibers, II–IV are EDS spectra of the elements contained at points A, B, and C. (b) Typical EDS microanalysis on selected areas of a single $TiO_2/SnO_2$ nanofiber. (a) Reproduced with permission (130) Copyright 2015, Royal Society of Chemistry; (b) adapted with permission (131) Copyright 2007, American Chemical Society.

Figure 11b. From the EDS results, it could be obviously found that one of the two small nanofibers corresponds to $SnO_2$ and the other to $TiO_2$.

### 4.2.2 Infrared spectroscopic analysis

Infrared spectroscopy was a common characterization method in materials science, and it also could be used for the identification of bicomponent fibers. Since different substances could selectively absorb the electromagnetic radiation in the infrared light area to perform structural analysis, the number, position, shape, and intensity of the sample bands were used to identify the type of fibers by comparing the spectrum of the standard sample.

Han et al. (132) prepared polyurethane (PU) (core)/polyurethane (PC) (shell) bicomponent nanofibers by using coaxial electrospinning technology and characterized their shell and core structures using infrared spectroscopy. Figure 12a shows the TEM image of the PU (core)/PC (shell) bicomponent fiber, and the obvious core/shell structure of the fiber can be seen. Figure 12b shows the infrared spectra of bicomponent fibers with different composite ratios, and Figure 11c shows the infrared spectra corresponding to single components. In Figure 12b, there are 2,965 $cm^{-1}$ (2,975–2,950 $cm^{-1}$) and

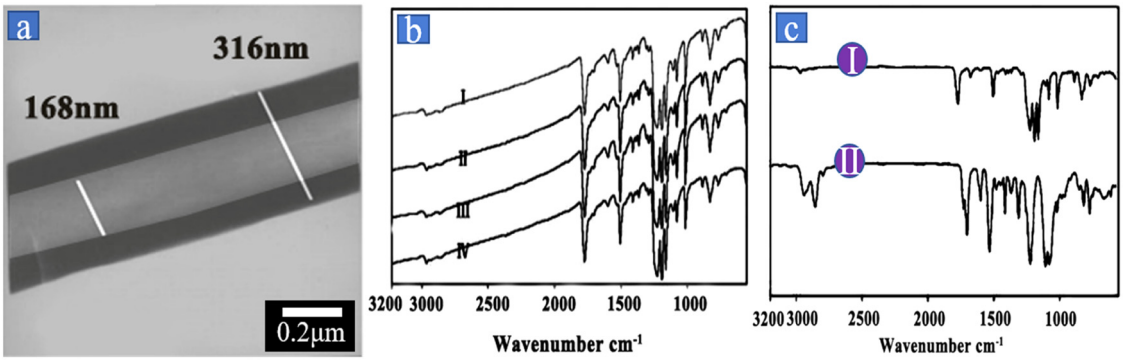


**Figure 12:** (a) TEM image of transmission electron microscopy of the PU (core)/PC (shell) fiber; (b) FT-IR spectra of various fiber samples of PU (core)/PC (shell): 20 wt%/4 wt%; 20 wt%/6 wt%; 20 wt%/8 wt%; and 20 wt%/10 wt%; (c) FT-IR spectra of various fiber samples (I: PC, II: PU). (a–c) Adapted with permission (132) Copyright 2008, Society of Plastics Engineers.

2,868 $cm^{-1}$ regions (2,885–2,860 $cm^{-1}$), reflecting the C–H asymmetric and symmetric flexing vibrations of alkyl ($-CH_3$), and its distortion caused 1,466 $cm^{-1}$ (1,470–1,435 $cm^{-1}$) and 1,386 $cm^{-1}$ regions (1,386–1,370 $cm^{-1}$). All of these regions correspond to the I-curve in Figure 12c, Thus, it is confirmed that PC existed in bicomponent fibers. From similar regions in Figure 12b, we compared the appearances of 2,937, 2,854, 1,730, 1,702, 1,479, 1,109, and 1,080 $cm^{-1}$ regions corresponding to the II-curve in Figure 12c, and thus confirmed the presence of PU polymer in the composite fiber. Therefore, the bicomponent fiber was confirmed.

However, for bicomponent fibers with a core/shell structure, the ability of infrared light penetration was poor so it might be not strong enough to completely pass through the shell and then reach the core. Consequently, the collected information was mainly the characteristic information of the shell material, and the information about the core material was weak.

### 4.2.3 DSC analysis

Differential scanning calorimeter (DSC) could reflect the thermal properties of the materials. Specific to the bicomponent fiber, the DSC results of a bicomponent fiber may be usually the superposition of the single-component polymers. Therefore, it was feasible to further confirm the composition of bicomponent fibers by comparing the positions of melting peaks (melting points) on the secondary heating curve in the DSC spectrum with the relative results of single-component fibers (133).

Rungiah et al. (134) prepared PP/PLA side-by-side bicomponent fibers using a melt blow process and characterized them by DSC. Figure 13a shows the SEM image of the as-spun side-by-side bicomponent fibers. Figure 13b shows the thermal curves of the PP/PLA fiber obtained by DSC analysis at a high air flow rate (300 $m^3 h^{-1}$, so PP/PLA is named as PP-PLA300). In Figure 13b, from the DSC images of PP, it can be seen that there is only one melting peak at 170°C and there is no sign of phase transition, indicating that PP had a crystal structure. There are two exothermic peaks, melting peak and glass transition peak (658°C) in the PLA curve, and two endothermic peaks are observed at 90°C and 150°C, which are related to the crystal phase transition of cold crystals and crystal phase transition from the beta to the alpha crystal form, respectively.

The thermogram of the PP/PLA bicomponent fiber shows the combination of PP and PLA single components,

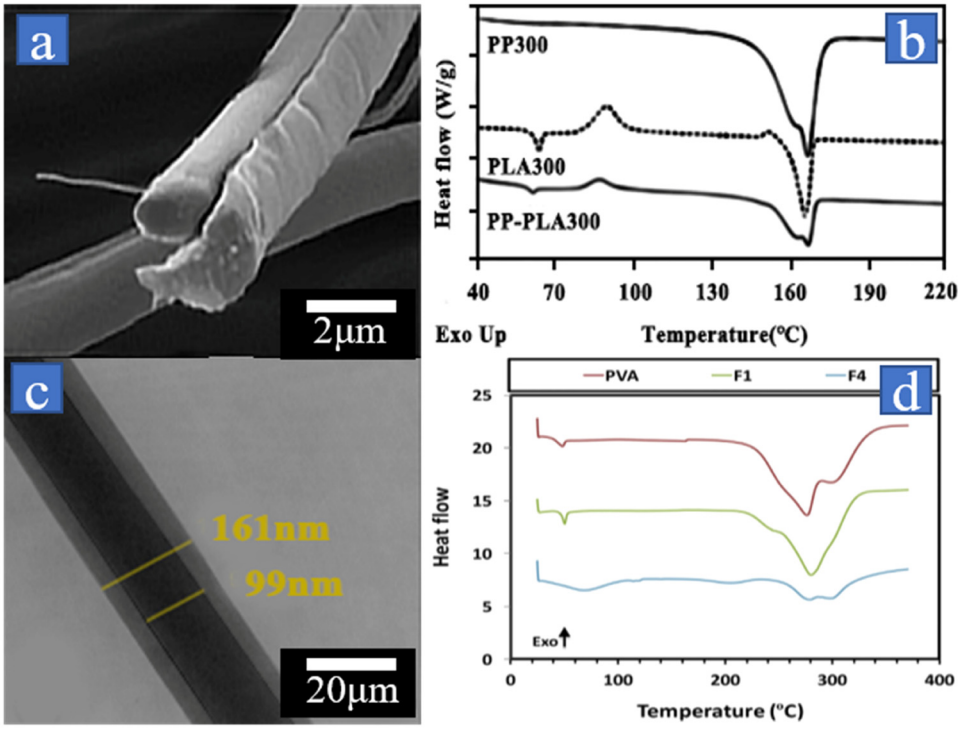


**Figure 13:** (a) SEM image of the cross section of a PP/PLA S/S filament (PP-PLA300), (b) DSC thermograph of PP, PLA monocomponent, and PP/PLA bicomponent melt-blown. (c) TEM images of electrospun nanofibers, (d) DSC thermograph of electrospun nanofibers. (a and b) Adapted with permission (134) Copyright 2016, Wiley Periodicals; (c and d) adapted with permission (135) Copyright 2019, Elsevier B.V.

and it could also be seen that the glass transition and crystallization peaks corresponded to the PLA map, but shifted to lower temperatures with minimal intensity, which was mainly due to the reduction of PLA components. From the results, it can be inferred that the side-by-side structure of the bicomponent fibers did not change much compared with the single component of the composition.

Mohammad et al. (135) had fabricated a core/shell nanofiber with PVA: Rosuvastatin (RSV) as the core and silk fibroin (SF) as the shell and analyzed and characterized their components using DSC. The TEM image in Figure 13c ensures its core/shell structure, and Figure 13d shows the DSC curves of pure PVA, PVA-RSV (F1; core part), and core/shell SF/PVA-RSV nanofibers (F4). It was found that the PVA DSC spectrum showed $T_g$ at 41°C and endothermic peaks at 48°C, 275°C, and 305°C; the former was related to water evaporation, and the latter peak can be attributed to the thermal degradation of PVA. While, for the F1 sample, the $T_g$ of PVA shifted to a higher temperature ($T_g \approx 49$°C), indicating successful hydrogen bonding of RSV to PVA; in addition, the core/shell nanofibers (in the F4 sample) clearly showed two different $T_g$ values at 49°C (PVA) and 191°C (SF), while the F1 sample showed only one $T_g$ at 49°C. This result indicated the presence of two different phase structures in the nanofibers and the successful coverage of the core of PVA/RSV with the shell of SF.

## 4.3 Other identification methods

The abovementioned identification methods were suitable in the situation that there was no chemical reaction between the two components in the bicomponent fibers. However, if some reaction occurred between the components, a reaction product would be generated and locked at the interface between the two components. Another method may be needed to identify the bicomponent fibers (136).

Zhao et al. (137) had prepared poly(L-lactic acid) (PLLA)/poly(D-lactic acid) (PDLA) bicomponent fibers by the side-by-side electrospinning process by selecting PLLA and PDLA in a 1:1 ratio. The prepared bicomponent fibers were characterized by diameter measurements, XRD, and FTIR spectroscopy.

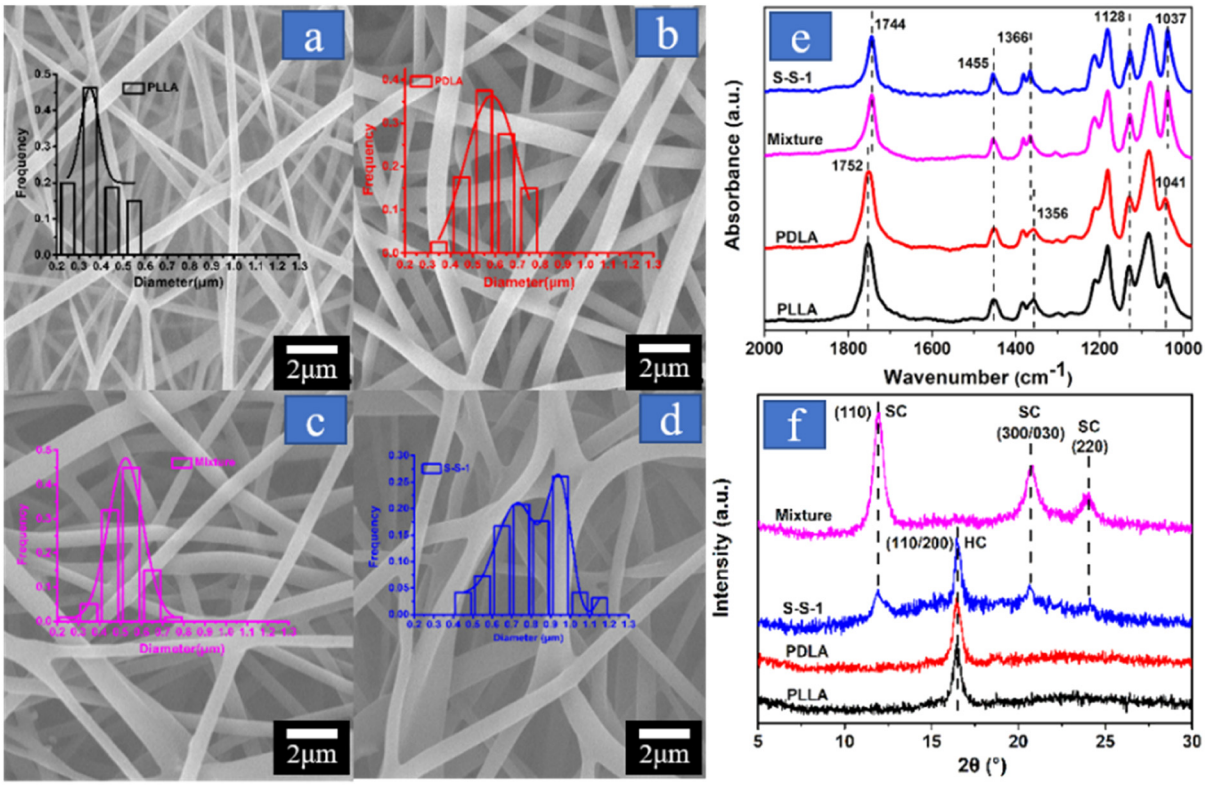


**Figure 14:** SEM micrographs and diameter distribution of (a) PLLA, (b) PDLA, (c) PLLA/PDLA mixture, and (d) S-S-1 bicomponent nanofibers. (e) FT-IR spectra of PLLA, PDLA, S-S-1 bicomponent, and PLLA/PDLA mixture nanofibers. (f) X-ray diffraction profiles of PLLA, PDLA, S-S-1 bicomponent, and PLLA/PDLA mixture nanofibers. Reproduced with permission (137) Copyright Wiley-VCH Verlag GMBH & Co. KGaA.

As shown in Figure 14a–d, the diameter distribution of 100 randomly selected fibers for each sample was measured. For the single-component fibers, their diameter distribution presented a continuous monotonic distribution, while the bicomponent fibers presented a bimodal distribution. For PLLA, PDLA, and PLLA/PDLA mixed electrospun fibers, the peak diameters were 373.5, 578.5, and 516.8 nm, respectively (see Figure 14a–c); while the bimodal diameter of PLLA/PDLA bicomponent fibers was approximately 730 and 950 nm as shown in Figure 14d. The lower peak diameter was the single-component fiber separated from the main body, and the higher peak diameter might respond to the bicomponent fiber. The diameter distribution may support the as-spun fiber with a side-by-side structure.

To examine the components of the as-spun fibers, FTIR spectra were measured. As shown in Figure 14e, the peak value of 1,037 $cm^{-1}$ in the side-by-side bicomponent fiber indicated that not only the molecular stereocomplexation between PLLA and PDLA existed, but also the stereo-complex crystal structure was formed in the bicomponent fibers and the interaction between the enantiomeric chains formed by the stereo-complex drive the nucleation in sc-crystals. The XRD patterns of the four different types of fibers are shown in Figure 14f, and the diffraction peaks at $2\theta = 11.9°$, 20.7°, and 24.1° correspond to the diffractions of the (110), (300/030), and (220) planes of the sc-crystal, respectively. It was found that the XRD patterns of the side-by-side bicomponent nanofibers with syringe speed of 1 mL $h^{-1}$ (S-S-1 bicomponent nanofibers) had characteristic diffraction peaks of HC and SC crystals, which fully demonstrated the presence of crystalline sandwich structures in the bicomponent nanofibers. These results indicated that the reaction occurred during the side-by-side electrospinning process between the two single components.

## 5 Conclusion and perspectives

In conclusion, the bicomponent fibers mainly contained side-by-side, core/shell, and matrix/protofibril types, according to their cross-sectional shapes. To prepare these bicomponent fibers, spun bonding and electrospinning were the main methods used recently. Moreover, the identification of bicomponent fibers depended on their physical structures and chemical components.

Generally, examination of the cross-sectional shapes of the bicomponent fibers by using a microscope was the most common and convenient way to identify their physical structures. Meanwhile, the EDS analysis, FTIR spectra, and DSC analysis were the common methods to ensure their chemical components. Each of these methods had its own characteristics and scope of application for finding evidence for bicomponent fibers. In practice, a single method was not enough to identify the bicomponent fibers, and several methods including both physical and chemical ones were needed. Moreover, since more and more electrospun bicomponent fibers were fabricated, their smaller diameters, below 1 μm, may cause difficulty in examining the cross-sectional shape of the fibers, and therefore, fluorescence labeling and TEM may be the effective ways.

At present, the structure of bicomponent fibers was mostly a symmetrical structure and there were a few suitable materials. In the future, with in-depth research, the asymmetric structures would appear and the preparation technology would tend to be mature. More and more materials would be used for the preparation of bicomponent fibers, and their properties might be increasingly better, and the application fields could be much more extensive. Different types of new methods will be applied to identify the newly prepared bicomponent fibers. Moreover, for within the different types of bicomponent fibers, more attention was focused on the side-by-side and core/shell ones and INS structures might the next fashion, especially for electrospinning.

**Funding information:** This work was supported by the China Postdoctoral Science Foundation (2020M671998), the National Natural Science Foundation of China (51703102), and the State Key Laboratory of Bio-Fibers and Eco-Textiles Foundation (Qingdao University) No. ZKT35.

**Author contributions:** Shufang Zhu: writing – original draft, writing – review and editing, methodology, formal analysis; Xin Meng: formal analysis, visualization; Xu Yan: conceptualization, writing – review and editing, supervision, project administration, resources; Shaojuan Chen: supervision, resources.

**Conflict of interest:** The authors state no conflict of interest.

## References

(1) Van Dyk H, Peralta P, Peszlen I. Modeling of the mechanical properties of a wood-fiber/bicomponent-fiber composite. BioResources. 2013;8:3672–84. doi: 10.15376/biores.8.3.3672-3684.

(2) Geleji F, Druzsbaczky G. Bicomponent fiber structures on polypropylene basis. J Polym Sci. 2007;42:713–6. doi: 10.1002/polc.5070420222.
(3) Chen S, Jia F, Zhao L, Qiu F, Jiang S, Ji J, et al. Electrospun fiber membrane with asymmetric NO release for the differential regulation of cell growth. Bio-Des Manuf. 2021;4:469–78. doi: 10.1007/s42242-021-00131-w.
(4) Jiang X, Bai Y, Chen X, Liu W. A review on raw materials, commercial production and properties of lyocell fiber. J Bioresour Bioprod. 2020;5:16–25. doi: 10.1016/j.jobab.2020.03.002.
(5) Liu L, Xu W, Ding Y, Agarwal S, Greiner A, Duan G. A review of smart electrospun fibers toward textiles. Compos Commun. 2020;22:100506. doi: 10.1016/j.coco.2020.100506.
(6) Ewulonu C, Liu X, Wu M, Yong H. Lignin-containing cellulose nanomaterials: a promising new nanomaterial for numerous applications. J Bioresour Bioprod. 2019;4:3. doi: 10.10.21967/jbb.v4i1.186.
(7) Yao K, Chen J, Li P, Duan G, Hou H. Robust strong electrospun polyimide composite nanofibers from a ternary polyamic acid blend. Compos Commun. 2019;15:92–5. doi: 10.1016/j.coco.2019.07.001.
(8) Azmin SNHM, Hayat NAbM, Nor MSM. Development and characterization of food packaging bioplastic film from cocoa pod husk cellulose incorporated with sugarcane bagasse fibre. J Bioresour Bioprod. 2020;5:248–55. doi: 10.1016/j.jobab.2020.10.003.
(9) Yang X, Wang J, Guo H, Liu L, Xu W, Duan G. Structural design toward functional materials by electrospinning: a review. e-Polymers. 2020;20:682–712. doi: 10.1515/epoly-2020-0068.
(10) Gupta B, George W. A theory of self-crimping bicomponent filaments. Text Res J. 1975;45:338–49. doi: 10.1177/004051757504500412.
(11) Naeimirad M, Zadhoush A, Kotek R, Esmaeely Neisiany R, Nouri Khorasani S, Ramakrishna S. Recent advances in core/shell bicomponent fibers and nanofibers: a review. J Appl Polym Sci. 2018;135:46265. doi: 10.1002/app.46265.
(12) Hufenus R, Affolter C, Camenzind M, Reifler FA. Design and characterization of a bicomponent melt-spun fiber optimized for artificial turf applications. Macromol Mater Eng. 2013;298:653–63. doi: 10.1002/mame.201200088.
(13) Tallury S, Pourdeyhimi B, Pasquinelli M, Spontak R. Physical microfabrication of shape-memory polymer systems via bicomponent fiber spinning. Macromol Rapid Commun. 2016;37:1837–43. doi: 10.1002/marc.201600235.
(14) Yan X, Yu M, Ramakrishna S, Russell S, Long Y. Advances in portable electrospinning devices for in situ delivery of personalized wound care. Nanoscale. 2019;11:19166–78. doi: 10.1039/c9nr02802a.
(15) Cai M, He H, Zhang X, Yan X, Li J, Chen F, et al. Efficient synthesis of PVDF/PI side-by-side bicomponent nanofiber membrane with enhanced mechanical strength and good thermal stability. Nanomaterials (Basel). 2018;9:39. doi: 10.3390/nano9010039.
(16) Houis S, Schmid M, Lübben J. New functional bicomponent fibers with core/sheath-configuration using poly(phenylene sulfide) and poly(ethylene terephthalate). J Appl Polym Sci. 2007;106:1757–67. doi: 10.1002/app.26846.
(17) Chiu Y, Tseng H, Lo Y, Wu B, Chen J. Plateau-rayleigh instability morphology evolution (PRIME): from electrospun core-shell polymer fibers to polymer microbowls. Macromol Rapid Commun. 2017;38:1600689. doi: 10.1002/marc.201600689.
(18) Wu H, Bian F, Gong R, Zeng Y. Effects of electric field and polymer structure on the formation of helical nanofibers via coelectrospinning. Ind Eng Chem Res. 2015;54:9585–90. doi: 10.1021/acs.iecr.5b02882.
(19) Reddy K, Nakata K, Ochiai T, Murakami T, Tryk D, Fujishima A. Nanofibrous $TiO_2$-core/conjugated polymer-sheath composites: synthesis, structural properties and photocatalytic activity. J Nanosci Nanotechnol. 2010;10:7951–7. doi: 10.1166/jnn.2010.3143.
(20) Tang Q, Fang L, Guo W. Effects of bamboo fiber length and loading on mechanical, thermal and pulverization properties of phenolic foam composites. J Bioresour Bioprod. 2019;4:51–9. doi: 10.21967/jbb.v4i1.184.
(21) Yu D, Branford-White C, Bligh S, White K, Chatterton N, Zhu L. Improving polymer nanofiber quality using a modified coaxial electrospinning process. Macromol Rapid Commun. 2011;32:744–50. doi: 10.1002/marc.201100049.
(22) Leal A, Naeimirad M, Gottardo L, Schuetz P, Zadhoush A, Hufenus R. Microfluidic behavior in melt-spun hollow and liquid core fibers. Int J Polym Mater Po. 2016;65:451–6. doi: 10.1080/00914037.2015.1129957.
(23) Joseph B, Sagarika V, Sabu C, Kalarikkal N, Thomas S. Cellulose nanocomposites: fabrication and biomedical applications. J Bioresour Bioprod. 2020;5:223–37. doi: 10.1016/j.jobab.2020.10.001.
(24) Cai M, Yuan D, Zhang X, Pu Y, Liu X, He H, et al. Lithium ion battery separator with improved performance via side-by-side bicomponent electrospinning of PVDF-HFP/PI followed by 3D thermal crosslinking. J Power Sources. 2020;461:228123. doi: 10.1016/j.jpowsour.2020.228123.
(25) Zhao X, Wang X, Lou T. Preparation of fibrous chitosan/sodium alginate composite foams for the adsorption of cationic and anionic dyes. J Hazard Mater. 2021;403:124054. doi: 10.1016/j.jhazmat.2020.124054.
(26) Wang H, Zhang J, Ning X, Tian M, Long Y, Ramakrishna S. Recent advances in designing and tailoring nanofiber composite electrolyte membranes for high-performance proton exchange membrane fuel cells. Int J Hydrog Energy. 2021;46:25225–51. doi: 10.1016/j.ijhydene.2021.05.048.
(27) Jian S, Tian Z, Zhang K, Duan G, Yang W, Jiang S. Hydrothermal synthesis of Ce-doped ZnO heterojunction supported on carbon nanofibers with high visible light photocatalytic activity. Chem Res Chin Univ. 2021;37:565–70. doi: 10.1007/s40242-021-1114-6.
(28) Wang X, Gong R. Thermally bonded nonwoven filters composed of bi-component polypropylene/polyester fiber. II. Relationships between fabric area density, air permeability, and pore size distribution. J Appl Polym Sci. 2006;102:2264–75. doi: 10.1002/app.24169.
(29) Yue X, Jia Y, Wang X, Zhou K, Zhai W, Zheng G, et al. Highly stretchable and durable fiber-shaped strain sensor with porous core-sheath structure for human motion monitoring. Compos Sci Technol. 2020;189:108038. doi: 10.1016/j.compscitech.2020.108038.
(30) Wang T, Ji X, Jin L, Feng Z, Wu J, Zheng J, et al. Fabrication and characterization of heparin-grafted poly-L-lactic acid-chitosan core-shell nanofibers scaffold for vascular gasket. ACS

Appl Mater Interfaces. 2013;5:3757–63. doi: 10.1021/am400369c.
(31) Yan E, Fan Y, Sun Z, Gao J, Hao X, Pei S, et al. Biocompatible core-shell electrospun nanofibers as potential application for chemotherapy against ovary cancer. Mater Sci Eng C Mater Biol Appl. 2014;41:217–23. doi: 10.1016/j.msec.2014.04.053.
(32) Lund A, Hagström B. Melt spinning of β-phase poly(vinylidene fluoride) yarns with and without a conductive core. J Appl Polym Sci. 2011;120:1080–9. doi: 10.1002/app.33239.
(33) Zhang Z, Tu W, Peijs T, Bastiaansen C. Fabrication and properties of poly(tetrafluoroethylene) nanofibres via sea-island spinning. Polymer. 2017;109:321–31. doi: 10.1016/j.polymer.2016.12.060.
(34) Han Q, Li J, Huang W. Deformation kinetics of PET/I-PP sea-island conjugate fibers in laser-heated flow drawing. Adv Mat Res. 2012;627:307–11. doi: 10.4028/www.scientific.net/AMR.627.307.
(35) Sugawara K, Ikaga T, Kim K, Ohkoshi Y, Okada K, Masunaga H, et al. Fiber structure development in PS/PET sea-island conjugated fiber during continuous laser drawing. Polymer. 2015;79:37–46. doi: 10.1016/j.polymer.2015.10.006.
(36) Zhao R, Wadsworth LC, Sun C, Zhang D. Properties of PP/PET bicomponent melt blown microfiber nonwovens after heat-treatment. Polym Int. 2003;52:133–7. doi: 10.1002/pi.1070.
(37) Chen S, Liu G, He H, Zhou C, Yan X. Physical structure induced hydrophobicity analyzed from electrospinning and coating polyvinyl butyral films. Adv Cond Matter Phys. 2019;2019:1–5. doi: 10.1155/2019/6179456.
(38) Dai Z, Yan F, Qin M, Yan X. Fabrication of flexible $SiO_2$ nanofibrous yarn via a conjugate electrospinning process. e-Polymers. 2020;20:600–5. doi: 10.1515/epoly-2020-0063.
(39) Nayak R, Padhye R, Kyratzis I, Truong Y, Arnold L. Recent advances in nanofibre fabrication techniques. Text Res J. 2011;82:129–47. doi: 10.1177/0040517511424524.
(40) Dong W, Liu J, Mou X, Liu G, Huang X, Yan X, et al. Performance of polyvinyl pyrrolidone-isatis root antibacterial wound dressings produced in situ by handheld electrospinner. Colloid Surf B. 2020;188:110766. doi: 10.1016/j.colsurfb.2019.110766.
(41) Liu G, Yan X, Yan F, Chen F, Hao L, Chen S, et al. In situ electrospinning iodine-based fibrous meshes for antibacterial wound dressing. Nanoscale Res Lett. 2018;13:309. doi: 10.1186/s11671-018-2733-9.
(42) Chien A, Gulgunje P, Chae H, Joshi A, Moon J, Feng B, et al. Functional polymer–polymer/carbon nanotube bi-component fibers. Polymer. 2013;54:6210–7. doi: 10.1016/j.polymer.2013.08.061.
(43) Gupta P, Wilkes G. Some investigations on the fiber formation by utilizing a side-by-side bicomponent electrospinning approach. Polymer. 2003;44:6353–9. doi: 10.1016/s0032-3861(03)00616-5.
(44) Peng H, Xie R, Fang K, Cao C, Qi Y, Ren Y, et al. Effect of diethylene glycol on the inkjet printability of reactive dye solution for cotton fabrics. Langmuir. 2021;37:1493–500. doi: 10.1021/acs.langmuir.0c03016.
(45) Wang H, Wang X, Fan T, Zhou R, Li J, Long Y, et al. Fabrication of electrospun sulfonated poly(ether sulfone) nanofibers with amino modified $SiO_2$ nanosphere for optimization of nanochannels in proton exchange membrane. Solid State Ion. 2020;349:115300. doi: 10.1016/j.ssi.2020.115300.
(46) Zhang L. Development and application of bi-component fiber. Synth Technol Application. 2004;19:38–41.
(47) Zhang C, Zhou J, Wang R, Dong Z. Crystallinity and thermal shrinkage properties of COPEET_HSPET side-by-side bicomponent fiber. China Synth Fiber Ind. 2015;38:24. doi: 10.3969/j.issn.1001-0041.2015.01.006.
(48) Lin T, Wang H, Wang X. Self-crimping bicomponent nanofibers electrospun from polyacrylonitrile and elastomeric polyurethane. Adv Mater. 2005;17:2699–703. doi: 10.1002/adma.200500901.
(49) Oh T, Han S, Lyoo W, Khil M. Annealing effects on molecular structures and physical properties of side-by-side conjugate fibers. Text Res J. 2011;81:2065–71. doi: 10.1177/0040517511416278.
(50) Zhang D, Sun C, Wadsworth L. Modeling the mono-and bicomponent fiber meltblown process with surface response methodology. Text Res J. 2016;71:301–8. doi: 10.1177/004051750107100404.
(51) Zhao L, Hu H, Shen J, Rong H. The use of a polytrimethylene terephthalate/polyester bi-component filament for the development of seamless garments. Text Res J. 2013;83:1283–96. doi: 10.1177/0040517512471749.
(52) Yan X, Yu M, Zhang L, Jia X, Li J, Duan X, et al. A portable electrospinning apparatus based on a small solar cell and a hand generator: design, performance and application. Nanoscale. 2016;8:209–13. doi: 10.1039/c5nr06858d.
(53) Yan Y, Zhu F, Sun H, Chen P, Pan X, Chen X. Study on the properties of side-by-side composite fiber raw materials and fibers. Synth Technol Appl. 2019;34:36–40.
(54) Akers S, Kaufmann J, Schwitter E. Bi-component polyolefin fibers used for concrete and shotcrete applications. In Sustainable and nonconventional construction materials using inorganic bonded fiber composites; Woodhead Publishing, 2017. p. 445–52. doi: 10.1016/b978-0-08-102001-2.00019-xpp.
(55) Hufenus R, Reifler FA, Maniura-Weber K, Spierings A, Zinn M. Biodegradable bicomponent fibers from renewable sources: melt-spinning of poly(lactic acid) and poly[(3-hydroxybutyrate)-*co*-(3-hydroxyvalerate)]. Macromol Mater Eng. 2012;297:75–84. doi: 10.1002/mame.201100063.
(56) Zhang L, Wang J, Fuentes C, Zhang D, Van Vuure A, Seo J, et al. Wettability of carbon nanotube fibers. Carbon. 2017;122:128–40. doi: 10.1016/j.carbon.2017.06.027.
(57) Zhou F, Wu S, Rader C, Ma J, Chen S, Yuan X, et al. Crosslinked ionic alginate and cellulose-based hydrogels for photoresponsive drug release systems. Fiber Polym. 2020;21:45–54. doi: 10.1007/s12221-020-9418-6.
(58) Duan G, Bagheri A, Jiang S, Golenser J, Agarwal S, Greiner A. Exploration of macroporous polymeric sponges as drug carriers. Biomacromolecules. 2017;18:3215–21. doi: 10.1021/acs.biomac.7b00852.
(59) Zhou S, Zhou G, Jiang S, Fan P, Hou H. Flexible and refractory tantalum carbide-carbon electrospun nanofibers with high modulus and electric conductivity. Mater Lett. 2017;200:97–100. doi: 10.1016/j.matlet.2017.04.115.
(60) Duan G, Jin M, Wang F, Greiner A, Agarwal S, Jiang S. Core effect on mechanical properties of one dimensional electrospun core-sheath composite fibers. Compos Commun. 2021;25:100773. doi: 10.1016/j.coco.2021.100773.

(61) Ouyang W, Liu S, yao K, Zhao L, Cao L, Jiang S, et al. Ultrafine hollow $TiO_2$ nanofibers from core-shell composite fibers and their photocatalytic properties. Compos Commun. 2018;9:76–80. doi: 10.1016/j.coco.2018.06.006.
(62) El-Salmawy A, Miyamoto M, Kimura Y. Preparing a core-sheath bicomponent fiber of poly(butylene terephthalate)/poly(butylene succinate-*co*-L-lactate). Text Res J. 2016;70:1011–8. doi: 10.1177/004051750007001112.
(63) Demirci E, Acar M, Pourdeyhimi B, Silberschmidt V. Finite element modelling of thermally bonded bicomponent fibre nonwovens: tensile behaviour. Comput Mater Sci. 2011;50:1286–91. doi: 10.1016/j.commatsci.2010.02.039.
(64) Lu L, Xing D, Xie Y, Teh K, Zhang B, Chen S, et al. Electrical conductivity investigation of a nonwoven fabric composed of carbon fibers and polypropylene/polyethylene core/sheath bicomponent fibers. Mater Des. 2016;112:383–91. doi: 10.1016/j.matdes.2016.09.096.
(65) Vaikhanski L, Lesko JJ, Nutt SR. Cellular polymer composites based on bi-component fibers. Compos Sci Technol. 2003;63:1403–10. doi: 10.1016/s0266-3538(03)00087-3.
(66) Wang X, Gong R, Dong Z, Porat I. Frictional properties of thermally bonded 3D nonwoven fabrics prepared from polypropylene/polyester bi-component staple fiber. Polym Eng Sci. 2006;46:853–63. doi: 10.1002/pen.20525.
(67) Fan T, Su Y, Fan Q, Li Z, Cui W, Yu M, et al. Robust graphene@PPS fibrous membrane for harsh environmental oil/water separation and all-weather cleanup of crude oil spill by joule heat and photothermal effect. ACS Appl Mater Interfaces. 2021;13:19377–86. doi: 10.1021/acsami.1c04066.
(68) Sun Z, Zussman E, Yarin A, Wendorff J, Greiner A. Compound core–shell polymer nanofibers by co-electrospinning. Adv Mater. 2003;15:1929–32. doi: 10.1002/adma.200305136.
(69) Guo N, Huang X, Jing L. Application research of high-strength needled filter bag with sea-island superfine fiber. Adv Mat Res. 2014;1004–1005:553–6. doi: 10.4028/www.scientific.net/AMR.1004-1005.553.
(70) Gong R, Nikoukhesal A. Hydro-entangled bi-component microfiber nonwovens. Polym Eng Sci. 2009;49:1703–7. doi: 10.1002/pen.21400.
(71) Gulgunje P, Newcomb B, Gupta K, Chae H, Tsotsis T, Kumar S. Low-density and high-modulus carbon fibers from polyacrylonitrile with honeycomb structure. Carbon. 2015;95:710–4. doi: 10.1016/j.carbon.2015.08.097.
(72) Huang M, Chen K. Capability analysis for a multi-process product with bilateral specifications. Int J Adv Manuf Tech. 2003;21:801–6. doi: 10.1007/s00170-002-1396-x.
(73) Ma W, Liu L, Yang R, Zhang T, Zhang Z, Song L, et al. Monitoring a micromechanical process in macroscale carbon nanotube films and fibers. Adv Mater. 2009;21:603–8. doi: 10.1002/adma.200801335.
(74) Pan Z, Zhu M, Chen Y, Chen L, Wu W, Yu C, et al. The variation of fibrils' number in the sea-island fiber -low density polyethylene/polyamide 6. Fiber Polym. 2010;11:494–9. doi: 10.1007/s12221-010-0494-x.
(75) Purane S, Panigrahi N. Microfibres, microfilaments & their applications. Autex Res J. 2007;7:148–58.
(76) Suvari F, Ulcay Y, Pourdeyhimi B. Influence of sea polymer removal on sound absorption behavior of islands-in-the-sea spunbonded nonwovens. Text Res J. 2018;89:2444–55. doi: 10.1177/0040517518797332.
(77) Zhao B, Qian X, Qian Y, Duo Y, Feng Y, Fan J, et al. The application of hollow segmented-pie bicomponent spunbond hydro-entangled microfiber nonwovens for microfiber synthetic leather apparel. AATCC J Res. 2019;6:45–9. doi: 10.14504/ajr.6.S1.10.
(78) Chang H, Luo J, Gulgunje P, Kumar S. Structural and functional fibers. Ann Rev Mater Res. 2017;47:331–59. doi: 10.1146/annurev-matsci-120116-114326.
(79) Jing Zhang Y, Takarada W, Kikutani T. Fabrication of fiber-reinforced single-polymer composites through compression molding of bicomponent fibers prepared by high-speed melt spinning process. Sen'i Gakkaishi. 2015;71:172–9. doi: 10.2115/fiber.71.172.
(80) Srivastava Y, Marquez M, Thorsen T. Microfluidic electrospinning of biphasic nanofibers with Janus morphology. Biomicrofluidics. 2009;3:12801. doi: 10.1063/1.3009288.
(81) Chen S, Hou H, Hu P, Wendorff JH, Greiner A, Agarwal S. Effect of different bicomponent electrospinning techniques on the formation of polymeric nanosprings. Macromol Mater Eng. 2009;294:781–6. doi: 10.1002/mame.200900139.
(82) Jiang Z, Tijing L, Amarjargal A, Park CH, An K, Shon H, et al. Removal of oil from water using magnetic bicomponent composite nanofibers fabricated by electrospinning. Compos Part B-Eng. 2015;77:311–8. doi: 10.1016/j.compositesb.2015.03.067.
(83) Duan G, Liu S, Jiang S, Hou H. High-performance polyamide-imide films and electrospun aligned nanofibers from an amide-containing diamine. J Bioresour Bioprod. 2019;54:6719–27. doi: 10.1007/s10853-019-03326-w.
(84) Duan G, Greiner A. Air-blowing-assisted coaxial electrospinning toward high productivity of core/sheath and hollow fibers. Macromol Mater Eng. 2019;304:1800669. doi: 10.1002/mame.201800669.
(85) Molnar K, Jedlovszky-Hajdu A, Zrinyi M, Jiang S, Agarwal S. Poly(amino acid)-based gel fibers with pH responsivity by coaxial reactive electrospinning. Macromol Rapid Commun. 2017;38:1700147. doi: 10.1002/marc.201700147.
(86) Wang M. Development of composite spinning technology abroad. China Synth Fiber Ind. 1981;6:42–9.
(87) Liu W, Zhang J, Liu H. Conductive bicomponent fibers containing polyaniline produced via side-by-side electrospinning. Polym (Basel). 2019;11:954. doi: 10.3390/polym11060954.
(88) Kessick R, Tepper G. Microscale polymeric helical structures produced by electrospinning. Appl Phys Lett. 2004;84:4807–9. doi: 10.1063/1.1762704.
(89) Chen S, Hou H, Hu P, Wendorff J, Greiner A, Agarwal S. Polymeric nanosprings by bicomponent electrospinning. Macromol Mater Eng. 2009;294:265–71. doi: 10.1002/mame.200800342.
(90) Gan X, Liu N, Ma X, Liu Q, Yang C. Study on the co-extrusion process morphology and performance of skin-core bicomponent fiber. Adv Mat Res. 2011;332–334:553–9. doi: 10.4028/www.scientific.net/AMR.332-334.553.
(91) Dasdemir M, Maze B, Anantharamaiah N, Pourdeyhimi B. Formation of novel thermoplastic composites using bicomponent nonwovens as a precursor. J Mater Sci. 2011;46:3269–81. doi: 10.1007/s10853-010-5214-9.
(92) Hada Y, Shikuma H, Ito H, Kikutani T. High-speed melt spinning of syndiotactic-polystyrene; improvement of spinnability and fiber structure development via bicomponent

spinning with atactic-polystyrene. J Macromol Sci B. 2007;44:549–71. doi: 10.1081/mb-200064814.
(93) Jiang S, Duan G, Zussman E, Greiner A, Agarwal S. Highly flexible and tough concentric triaxial polystyrene fibers. ACS Appl Mater Interfaces. 2014;6:5918–23. doi: 10.1021/am500837s.
(94) Kwak G, Lee G, Shim S, Yoon K. Fabrication of light-guiding core/sheath fibers by coaxial electrospinning. Macromol Rapid Commun. 2008;29:815–20. doi: 10.1002/marc.200800065.
(95) Li D, McCann J, Xia Y. Use of electrospinning to directly fabricate hollow nanofibers with functionalized inner and outer surfaces. Small. 2005;1:83–6. doi: 10.1002/smll.200400056.
(96) Lu Y, Xiao X, Mo J, Huan C, Qi S, Zhan Y, et al. Green nanoencapsulation technique for preparation of phase change nanofibers mats with core-sheath structure. Colloid Surf A. 2018;555:501–6. doi: 10.1016/j.colsurfa.2018.07.030.
(97) Yoon J, Yang H, Lee B, Yu W. Recent progress in coaxial electrospinning: new parameters, various structures, and wide applications. Adv Mater. 2018;30:e1704765. doi: 10.1002/adma.201704765.
(98) Liu H, Luo J, Chang H, Bakhtiary Davijani A, Wang P, Kumar S. Polyacrylonitrile sheath and polyacrylonitrile/lignin core bi-component carbon fibers. Carbon. 2019;149:165–72. doi: 10.1016/j.carbon.2019.04.004.
(99) Khatwani PA, Yardi SS. Bicomponent fibers: Fibers of modern era. Man Made Text India. 2003;46:19.
(100) Li D, Xia Y. Direct fabrication of composite and ceramic hollow nanofibers by electrospinning. Nano Lett. 2004;4:933–8. doi: 10.1021/nl049590f.
(101) He H, Chen L, Zhang Y, Hong S, Zhou Y, Zhu M. Studies on melt spinning of sea-island fibers. I. morphology evolution of polypropylene/polystyrene blend fibers. Fiber Polym. 2014;15:1941–9. doi: 10.1007/s12221-014-1941-x.
(102) Soltani I, Macosko C. Influence of rheology and surface properties on morphology of nanofibers derived from islands-in-the-sea meltblown nonwovens. Polymer. 2018;145:21–30. doi: 10.1016/j.polymer.2018.04.051.
(103) Wang D, Sun G, Chiou B. A high-throughput, controllable, and environmentally benign fabrication process of thermoplastic nanofibers. Macromol Mater Eng. 2007;292:407–14. doi: 10.1002/mame.200600460.
(104) Wang J, Sutti A, Wang X, Lin T. A new way to nanostructure hydrogels: electrospun thermo-responsive islands-in-the-sea nanofibres. MRS Proc. 2012;1403:Mrsf11-1403-v05-01. doi: 10.1557/opl.2012.418.
(105) Jingjit P, Srisawat N. Spinning of photocatalytic fiber as splittable segmented-pie bi-component fibers for antibacterial textiles. J Nanosci Nanotechnol. 2019;19:1554–61. doi: 10.1166/jnn.2019.16224.
(106) Prahsarn C, Klinsukhon W, Padee S, Suwannamek N, Roungpaisan N, Srisawat N. Hollow segmented-pie PLA/PBS and PLA/PP bicomponent fibers: an investigation on fiber properties and splittability. J Mater Sci. 2016;51:10910–16. doi: 10.1007/s10853-016-0302-0.
(107) Xu X, Zhang F, Wang W, Li N, Zhuang X, Wang H, et al. Development of amino acid-modified PET/PA6 segmented-pie bicomponent spunbonded microfiber nonwoven for bilirubin affinity adsorption. Fiber Polym. 2017;18:633–40. doi: 10.1007/s12221-017-6824-5.
(108) Zhou Y, Jiang L, Jia H, Xing X, Sun Z, Chen S, et al. Study on spinnability of PP/PU blends and preparation of PP/PU Bicomponent melt blown nonwovens. Fiber Polym. 2019;20:1200–7. doi: 10.1007/s12221-019-8111-0.
(109) Bazilevsky A, Yarin A, Megaridis C. Co-electrospinning of core-shell fibers using a single-nozzle technique. Langmuir. 2007;23:2311–4. doi: 10.1021/la063194q.
(110) An SL. Islands-and-sea spinning-ultrafinefiber-artificial leather. J Text Res. 2000;21:48–50.
(111) Ayad E, Cayla A, Rault F, Gonthier A, LeBlan T, Campagne C, et al. Influence of rheological and thermal properties of polymers during melt spinning on bicomponent fiber morphology. J Mater Eng Perform. 2016;25:3296–302. doi: 10.1007/s11665-016-2193-2.
(112) Cherif C, Tran N, Kirsten M, Bruenig H, Vogel R. Environmentally friendly and highly productive bi-component melt spinning of thermoregulated smart polymer fibres with high latent heat capacity. Express Polym Lett. 2018;12:203–14. doi: 10.3144/expresspolymlett.2018.19.
(113) Shu Y, Hsiao K. Physical characteristics and morphologies of PTT/m-iPP bi-component filaments of the island-in-sea type. J Polym Res. 2007;15:131–9. doi: 10.1007/s10965-007-9152-4.
(114) Zhao Y, Liu Y. The preparation of spunbonded PA6/PET segment bicomponent fiber. J Text Sci Eng. 2012;2:1–4. doi: 10.4172/2165-8064.1000106.
(115) Im Y, Oh T, Cha J, Seo Y, Hwang J, Nathanael J, et al. Preparation of poly(vinyl alcohol)/$ZrO_2$ composite nanofibers via co-axial electrospinning with higher $ZrO_2$ particle content. Fiber Polym. 2014;15:2066–71. doi: 10.1007/s12221-014-2066-.
(116) Yeom B, Pourdeyhimi B. Aerosol filtration properties of PA6/PE islands-in-the-sea bicomponent spunbond web fibrillated by high-pressure water jets. J Mater Sci. 2011;46:5761–7. doi: 10.1007/s10853-011-5531-7.
(117) Zhao Y, Cao X, Jiang L. Bio-mimic multichannel microtubes by a facile method. J Am Chem Soc. 2007;129:764–5. doi: 10.1021/ja068165g.
(118) Kim M, Jo S, Park J, Cho K. Flexible lateral organic solar cells with core–shell structured organic nanofibers. Nano Energy. 2015;18:97–108. doi: 10.1016/j.nanoen.2015.10.007.
(119) Liu X, Yang Y, Yu D, Zhu M, Zhao M, Williams G. Tunable zero-order drug delivery systems created by modified triaxial electrospinning. Chem Eng J. 2019;356:886–94. doi: 10.1016/j.cej.2018.09.096.
(120) Zhu C, Deng W, Pan J, Lu B, Zhang J, Su Q, et al. Structure effect of dual-spinneret on the preparation of electrospun composite nanofibers with side-by-side heterojunctions. J Mater Sci-Mater El. 2013;24:2287–91. doi: 10.1007/s10854-013-1091-8.
(121) Rajgarhia S, Benavides R, Jana S. Morphology control of bi-component polymer nanofibers produced by gas jet process. Polymer. 2016;93:142–51. doi: 10.1016/j.polymer.2016.04.018.
(122) Nguyen T, Chung O, Park J. Coaxial electrospun poly(lactic acid)/chitosan (core/shell) composite nanofibers and their antibacterial activity. Carbohydr Polym. 2011;86:1799–806. doi: 10.1016/j.carbpol.2011.07.014.

(123) Peng L, Jiang S, Seuß M, Fery A, Lang G, Scheibel T, et al. Two-in-one composite fibers with side-by-side arrangement of silk fibroin and poly(L-lactide) by electrospinning. Macromol Mater Eng. 2016;301:48–55. doi: 10.1002/mame.201500217.
(124) Gernhardt M, Peng L, Burgard M, Jiang S, Förster B, Schmalz H, et al. Tailoring the morphology of responsive bioinspired bicomponent fibers. Macromol Mater Eng. 2018;303:1700248. doi: 10.1002/mame.201700248.
(125) Wang L, Wang X, Chen B. Study of ultraviolet and extreme ultraviolet phosphors for imaging detector. Optical Technique. 2006;32:479–81. doi: 10.3321/j.issn:1002-1582.2006.z1.129.
(126) Lee K, Hwang S, Yoon J, Bhaskar S, Park T, Lahann J. Compartmentalized photoreactions within compositionally anisotropic Janus microstructures. Macromol Rapid Commun. 2011;32:431–7. doi: 10.1002/marc.201000558.
(127) Jin G, Lee S, Kim S, Kim M, Jang J. Bicomponent electrospinning to fabricate three-dimensional hydrogel-hybrid nanofibrous scaffolds with spatial fiber tortuosity. Biomed Microdevices. 2014;16:793–804. doi: 10.1007/s10544-014-9883-z.
(128) Lee K, Park T, Hwang S, Yoon J, Lahann J. Janus-core and shell microfibers. Langmuir. 2013;29:6181–6. doi: 10.1021/la4009416.
(129) Flynn K, O'Leary R, Roux C, Reedy B. Forensic analysis of bicomponent fibers using infrared chemical imaging. J Forensic Sci. 2006;51:586–96. doi: 10.1111/j.1556-4029.2006.00116.x.
(130) Chen G, Xu Y, Yu D, Zhang D, Chatterton N, White K. Structure-tunable Janus fibers fabricated using spinnerets with varying port angles. Chem Commun (Camb). 2015;51:4623–6. doi: 10.1039/c5cc00378d.
(131) Liu Z, Sun D, Guo P, Leckie J. An efficient bicomponent $TiO_2$/$SnO_2$ nanofiber photocatalyst fabricated by electrospinning with a side-by-side dual spinneret method. Nano Lett. 2007;7:1081–5. doi: 10.1021/nl061898e.
(132) Han X, Huang Z, He C, Liu L, Wu Q. Coaxial electrospinning of PC(shell)/PU(core) composite nanofibers for textile application. Polym Compos. 2006;27:381–7. doi: 10.1002/pc.20194.
(133) Zhang L, Hsieh Y. Nanoporous ultrahigh specific surface polyacrylonitrile fibres. Nanotechnology. 2006;17:4416–23. doi: 10.1088/0957-4484/17/17/022.
(134) Rungiah S, Ruamsuk R, Vroman P, Takarada W, Appert C, Jean C, et al. Structural characterization of polypropylene/poly(lactic acid) bicomponent meltblown. J Appl Polym Sci. 2017;134:44540. doi: 10.1002/app.44540.
(135) Kalani M, Nourmohammadi J, Negahdari B, Rahimi A, Sell S. Electrospun core-sheath poly(vinyl alcohol)/silk fibroin nanofibers with Rosuvastatin release functionality for enhancing osteogenesis of human adipose-derived stem cells. Mater Sci Eng C Mater Biol Appl. 2019;99:129–39. doi: 10.1016/j.msec.2019.01.100.
(136) Wang Z, He H, Liu G, Yan X, Ning X, Long Y. A newly reaction curing mechanism in conjugate electrospinning process. Mater Lett. 2019;254:5–8. doi: 10.1016/j.matlet.2019.07.010.
(137) Zhao R, He H, Cai M, Miao D, Yuan D, Ming J, et al. Nanocrystalline sandwich formed in polylactic acid fibers. Macromol Rapid Commun. 2019;40:e1900492. doi: 10.1002/marc.201900492.